Journal Name

ARTICLE TYPE

Cite this: DOI: 00.0000/xxxxxxxxxx

DFT Insights into Competing Mechanisms of Guaiacol Hydrodeoxygenation on a Platinum Cluster†

Chiara Nania,[a] Marco Bertini,[a] Laura Gueci,[a] Francesco Ferrante*[a] and Dario Duca[a]

Received Date
Accepted Date

DOI: 00.0000/xxxxxxxxxx

In a scenario of declining fossil resources and increasing demand for renewable and sustainable alternatives, biomass is the only source able to offer an easy and gradual transition in the use of current energy technologies based on the exploitation of carbon derivatives. Its conversion to liquid fuels has oriented our study towards the computational mechanistic analysis of the guaiacol catalytic hydrodeoxygenation, which is currently considered one of the most challenging routes for upgrading biomass-derived bio-oils. For this purpose, a subnanometric Pt_{10} platinum cluster was chosen as the catalyst model, being Pt a computational reference element for catalytic hydrogenation, and guaiacol as a model compound of bio-oils. DFT calculations revealed that the energy barriers related to the cleavage of $C(sp^2)$-O bonds in the direct deoxygenation mechanism are significantly lower (by an average of 60 kJ mol^{-1}) than those in the deoxygenation-through-hydrogenation mechanism in which $C(sp^3)$-O bond breaking from saturated ring occurs. Even if the ring hydrogenation is easier in the oxygenated compound, the analysis reveals that the direct deoxygenation mechanisms is favoured at all temperatures. Furthermore, the results obtained highlight that, from a thermodynamic perspective, the removal of oxygen groups preferentially occurs by the elimination of the $-OCH_3$ fragment as methanol and then of the $-OH$ fragment as a water molecule.

1 Introduction

Currently, fossil fuels are the main source of energy because of their good anti-knocking properties, high calorific and heating values; however, reserves are limited.[1,2] In this scenario, renewable energies sources offer a great potential to complement the depleting energy reserves and to significantly decrease the antropogenic greenhouse gas (GHG) emissions into the atmosphere.[1,3] Among alternative energy sources, lignocellulosic biomass (LC) has received amplified attention during the last decade because it represents the most abundant reservoir of renewable carbon that is easily accessible on earth.[4] It could provide a viable means of reducing the GHG impact of fossil fuels in the transportation sector.[1,5] Fast pyrolysis is a promising method to convert solid biomass into liquid bio-oils in the absence of oxygen.[6,7] However, the bio-oils produced by pyrolysis are a complex mixture of oxygenated components and, as such, have neither the chemical nor physical properties to compete with petroleum distillates as a transportation fuel.[8] However, their liquid form facilitates further processing making bio-oils key intermediates in the conversion of biomass to hydrocarbon products. Although these exhibit mainly cyclic structures, rather than linear chains as in petroleum, their use should not be limited by this characteristic.[9]

In this context, catalytic hydrodeoxygenation (HDO) is considered to be one of the most challenging process for LC biomass-derived bio-oils' upgrading.[10] Although a number of bio-oil HDO processes have been studied,[5,11] bio-oils derived from different feedstocks typically consist of more than 400 different organic compounds, which significantly complicates the study of catalytic activities and reaction pathways of the involved processes. Hence, it is important to select model compounds that represent the raw bio-oils for providing basic insight into the HDO process.

One of the most relevant aspects in the study of HDO concerns the order in which the hydrogenation and deoxygenation steps occur. Both of them are necessary to obtain biofuels, but deoxygenation has a primary role,difference actually involving the removal of oxygenated groups (such as $-OH$, $-OCH_3$) which are responsible for the instability of the bio-oils. Generally, two paths have been proposed for the hydrodeoxygenation mechanisms: (a) deoxygenation-through-hydrogenation (HYD) in which aromatic ring hydrogenation occurs first being, then, followed by the removal of oxygen via C-O hydrogenolysis from the satured hydrocarbon ring; (b) direct deoxygenation (DDO) which involves the cleavage of the Ar-O bond via hydrogenolysis before ring satura-

Dipartimento di Fisica e Chimica - Università degli Studi di Palermo, Viale delle Scienze Ed. 17, 90128 Palermo, Italy. Fax: +39 091 590015; Tel. +39 091 23897979; E-mail: francesco.ferrante@unipa.it

† Electronic Supplementary Information (ESI) available: Additional figures reporting elementary steps for HYD and DDO mechanisms (S1-S6). Gibbs free energies variations for all elementary steps; Gibbs free energies variations for molecules desorption. Detailed results from the application of modified Christiansen method. See DOI: 00.0000/00000000.

tion.[12–15]

Several catalysts have been applied for HDO of phenolic compounds,[16–18] e.g. metals supported on carbon nanostructures, zeolites, carbides, oxides, and even bifunctional catalysts[19–23] in which the synergic effect between the metal and acid sites seems to have a crucial role.

Regarding metal selection, it has been shown that the use of noble metals (e.g. Pt, Ru, Ir) provides high yields of hydrocarbons. However, owing to their high cost, there is a growing interest in non-noble metals, such as Ni and Co.[12,14,24–26] Murzin and coworkers actually claim that Ni-based catalysts can be considered an effective alternative to noble metals due to their low cost and dual functionality towards hydrogenation and hydrogenolysis.[27–30] Many studies suggest that the reaction pathway over noble metals is different from those occurring on other transition metal catalysts, and propose HYD mechanism as the predominant reaction pathway rather than DDO.[13,31]

Cluster catalysis, performed through metal or metal-containing systems with a definite numbers of atoms, is a research area that requires high sinergy between experimental and computational approaches.[23,32,33] The great variety of possible cluster structures, and their fluxionality, can be exploited to design new systems with tunable catalytic properties, defined by a proper choice of their sizes, shapes and dispersion degrees on a support.[19,21,34,35] In this broad context, the present work aims to study both the HYD and DDO mechanisms proposed for the hydrodeoxygenation of guaiacol on a subnanometric ten-atom platinum cluster. This in order to create a reference study for these kind of catalized reactions, showing data and descriptors that can be employed to evaluate the effects of customizing the catalytic model,as an example changing either the metal or the shape of the cluster, or fixing the latter on a given support.

2 Models and Computational Details

2.1 Models

A cluster of platinum with ten atoms, having tetrahedral symmetry and spin multiplicity 9,[36,37] was chosen as a representative of catalytic species consisting of subnanometer-sized clusters. Its structure, represented in Figure 1, shows the presence of atoms with different coordination: the four atoms at the top of the cluster have coordination number three, the remaining six atoms have coordination number six. Pt_{10} is topologically relatable to a tetra-capped octahedron: six atoms form an octahedron whose triangular faces alternately show a cap, i.e. they have an additional atom arranged perpendicular to the center of the face itself. This geometry is the result of global optimization of Pt clusters up to ten atoms, as reported by Demiroglu et al.[37] Among the subnanometer clusters, Pt_{10} exhibits large stability due to the number of its valence electrons that allow it to be filled with multiple electronic shells (magic number).[38] In its optimized structure Pt_{10} has average Pt-Pt bond lenghts of 2.71 Å and a cohesive energy of 275.4 kJ mol^{-1}. The hypotheses that both the hydrogen molecule fragmentation and H-atom diffusion among the catalyst sites are very easy processes were already tested in other investigations.[20,34,39] As a matter of fact DFT calculations revealed that hydrogen atoms can reach any configuration in the cluster and that the diffusion phenomena have to be considered essentially barrier-free when compared with the activation barriers typical of the HDO reaction.[40]

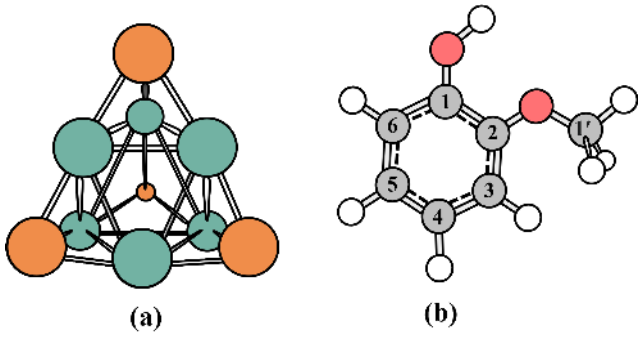

Fig. 1 (a) The Pt_{10} cluster used as subnanometric catalyst model; (b) the guaiacol molecule, whose atoms are numbered according to IUPAC rules. In the cluster, the orange and aquamarine colors indicate the coordination sites 3 and 6, respectively.

Guaiacol (2-methoxyphenol), a component of celery seed, tobacco leaf, orange leaf and lemon peel essential oils, was chosen as catalytic substrate.[41] It is an interesting compound for HDO mechanism studies since the $-OH$ and $-OCH_3$ groups are representative of a large number of oxygen-containing components in lignin-derived bio-oils, such as eugenol and vanillin.[42–45]

2.2 Computational details

All calculations were performed in the framework of DFT, using Gaussian 16 package.[46] DFT calculations were carried out using the B3LYP hybrid exchange correlation functional,[47] to which the D3 correction scheme, developed by Grimme, was added to account for dispersion interactions.[48] The lanl2dz basis set of Hay and Wadt[49,50] was used for each calculation. It employs Dunning's basis set (D95)[51] for light atoms (H, C, and O) and, for platinum, a double-zeta valence basis set associated to a pseudopotential. Polarization functions consisting of primitive Gaussians having angular momentum and exponents in accordance with the following scheme were added to the D95 basis set: H(s: 0.049, p:0.587), C (p: 0.0311, d:0.587), and O (p:0.0673, d:0.961). These functions were retrieved from the EMSL Basis Set Exchange website.[52]

The nature of minima and transition states on the reaction paths was revealed by inspection of the harmonic vibrational frequencies, checking that no imaginary frequencies are present in structures corresponding to minima in the potential energy surfaces, and only one imaginary frequency is present in transition state structures. The energetics of the reaction will be given in terms of vibrational zero-point corrected energy (E_{ZPV}); the desorption energies of stable products have been corrected for the basis set superposition error (BSSE) by using the counterpoise method of Boys and Bernardi.[53] Since BSSE was calculated as correction to the SCF energy, it will be reported in parenthesis along with the uncorrected E_{ZPV}.

3 Results and discussion

In the present investigation both the proposed mechanisms for the guaiacol HDO process were studied in order to evaluate whether deoxygenation occurs more readily from guaiacol, by breaking a $C(sp^2)-OH/OCH_3$ bond (DDO), or from 2-methoxycyclohexanol, through the cleavage of a $C(sp^3)-OH/OCH_3$ bond (HYD). In addition, it was aimed even to investigate the formation of secondary products, which might deactivate the catalyst by consequently reducing its activity and selectivity, or whose formation could be considered of special interest in other production processes. Ultimately, the mapping of the HDO process of guaiacol allows us to compare the same process on the isoeugenol species, which was studied at the same computational level and with the same catalyst, in order to understand whether structurally similar molecules may have a correspondingly similar reactive patterns.[40]

It is worth to note that other pathways could connect guaiacol to cyclohexane, including those where intermediates originating from dehydrogenation reactions (*i.e.* of the methyl or hydroxyl group) are involved.[54] To these could be added the high number of transformations a molecule such as guaiacol can undergo.[12,55] Here we actually considered only the direct defunctionalization reactions, from both the guaiacol (fully unsaturated phenyl ring) and 2-methoxycyclohexan-1-ol (fully saturated ring) molecules.

The selected HYD and DDO mechanisms of guaiacol on Pt_{10} will be discussed in detail below, presenting the reaction profiles of the elementary stages and providing the energetics associated with each process (such as energy barriers and desorption energies).

3.1 HYD mechanism

The HYD mechanism of guaiacol involves the hydrogenation of the benzene ring with the formation of 2-methoxycyclohexan-1-ol and the subsequent removal of the oxygenated groups ($-OCH_3$ and $-OH$); from 2-methoxycyclohexan-1-ol, depending on the order and chemical form whereby the oxygenated components are removed, three different pathways arise (Scheme 1): (1) removal of the $-OCH_3$ group as CH_3OH, leading to cyclohexanol, whence cyclohexane is obtained by loss of H_2O; (2) removal of the $-OH$ group as water and subsequent formation of methoxycyclohexane from which, by removal of CH_3OH or CH_4 and water, the cyclohexane is obtained; and (3) removal of the methyl group as CH_4 from the OCH_3 fragment with formation of cyclohexane-1,2-diol, finally yielding cyclohexane through the elimination of two water molecules.

Hydrogenation of the benzene ring follows a *Horiuti-Polanyi*[56] scheme involving the consecutive addition of hydrogen adatoms. Since the carbon atoms of the ring are not equivalent due to electronic effects of substituents and metal/substrate interactions that sometimes generate metastable geometries with increased reactivity, each carbon atom of the ring was considered, at least for the addition of the first hydrogen atom, to be a potentially reactive hence hydrogenable site. Based on kinetic and thermodynamic criteria, respectively governed by lower energy barrier and higher relative stability of the intermediate in the involved stage,

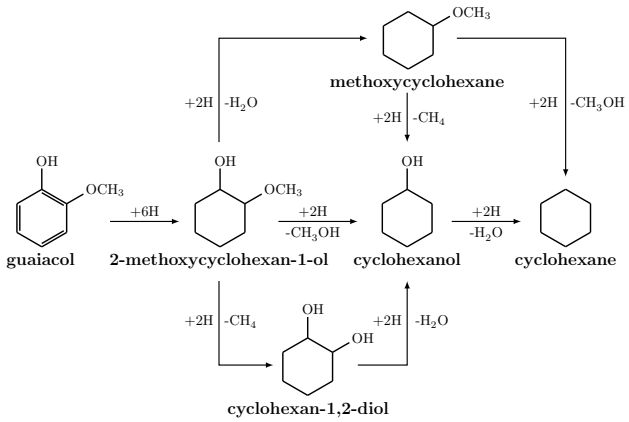

Scheme 1 Guaiacol conversion to cyclohexane according to HYD mechanism: schematic routes

the first hydrogen atom showed to be preferentially added on C6 (Figure 2). For the addition of the subsequent hydrogen atoms, we considered as potential sites for hydrogen attachment only the carbon atoms in *ortho* to the progressively added hydrogen atoms. As a matter of fact, as evidenced in experimental studies conducted on the hydrogenation of benzene[56–58] and in our previous computational work,[40] these carbon atoms appear to be activated by the vicinal presence of a hydrogen atom. On this basis, from intermediate I, the addition of a second H atom on the C1 and C5 centers was considered. The species preferentially obtained is 2-methoxycyclohexa-2,4-dien-1-ol (**II**; energy barrier of 88.2 kJ mol^{-1} for hydrogenation of C1 and desorption energy of 273.2 kJ mol^{-1} with BSSE = 28.0 kJ mol^{-1}), which, by addition of a third H atom to C5 of the ring, leads to intermediate **III**. By virtue of a lower energy barrier of about 16 kJ mol^{-1}, addition of the fourth hydrogen atom occurs preferentially on C2 leading to the 2-methoxycyclohex-3-en-1-ol (**IV**; desorption energy of 158.2 (BSSE = 22.4) kJ mol^{-1}). From this one, the last carbon atoms of the ring (C3 and C4) were considered as potential sites available for hydrogenation. Both the energy barrier (26.2 *vs* 34.3 kJ mol^{-1}) and the relative stability of the resulting intermediate (-18.5 *vs* 24.2 kJ mol^{-1}) suggest that the addition of the fifth hydrogen occurs preferentially on C4 leading, by successive addition of the last H atom to C3, to the 2-methoxycyclohexan-1-ol species (**VI**), whose desorption energy is 102.3 (BSSE = 19.0) kJ mol^{-1}.

Once the benzene ring was fully hydrogenated, the investigation of the final HYD paths, in order to get the whole conversion product, could be taken into account.

The first route (pathway 1) involves the formation of cyclohexane through the removal of $-OCH_3$ as methanol and the subsequent removal of $-OH$ as water. Therefore, the first elementary step entails cleavage of the C2-O bond and adsorption of the OCH_3 fragment on the upper portion of a side edge of the cluster. The cleavage is characterized by an energy barrier of 137.7 kJ mol^{-1} and leads to the (int1+CH_3O)/Pt_{10} species with an energy release of 66.5 kJ mol^{-1} (Figure 3).

In order to proceed with HDO reaction, a new H_2 molecule was fragmented on the cluster (Figure S1 of ESI†); thus the resulting (int1+CH_3O)/Pt_{10}2H species was used as a reactant for

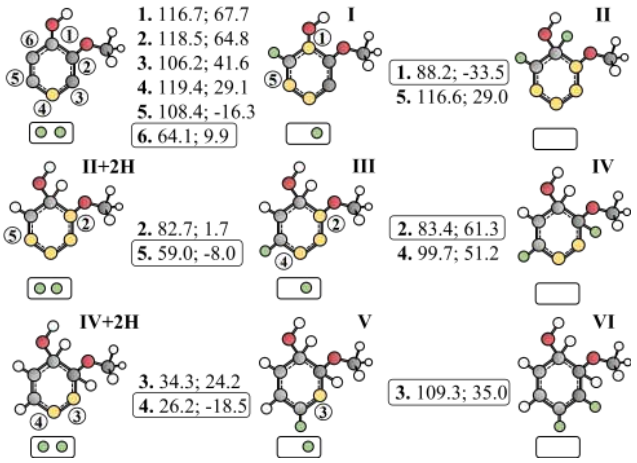

Fig. 2 Representation of the complete saturation of the aromatic ring of the guaiacol species adsorbed on the Pt_{10} cluster. In the molecular species, the yellow circles indicate the interaction sites of the molecule itself with the cluster, which is instead represented by a small rectangle containing the adsorbed hydrogen atoms (green circles). To the right of each species, the first number indicates the position where the catalytic hydrogen is added, the second is the energy barrier and the third is the reaction energy, both referred to the reactant of the elementary step. All energy values are expressed in kJ mol^{-1}. The first catalytic hydrogenation starts from guaiacol, the second from II+2H (2-methoxycyclohexa-2,4-dien- 1-ol), and the last from IV+2H (2-methoxycycloes-3-en-1- ol).

the formation of chemisorbed methanol, whose desorption energy was calculated to be equal to 91.9 kJ mol^{-1}, with BSSE = 8.8 kJ mol^{-1}. Following the desorption of methanol, there is the diffusion of an H atom through the cluster sites towards the unsaturated C2 atom of the ring. From the resulting species, (int1+CH_3O)/Pt_{10}H, there is a shift of an H atom to C2 of the ring (energy barrier of 106.5 kJ mol^{-1}) with formation of the adsorbed cyclohexanol, which is less stable than the reactant species of 43.3 kJ mol^{-1}. Cyclohexanol could desorb from the cluster with an energy of 117.8 (BSSE = 16.9) kJ mol^{-1}, representing a secondary reaction product. In the main reaction pathway, however, cyclohexanol/Pt_{10} undergoes C1-O bond cleavage. The elementary stage involved is characterized by a very high energy barrier of 192.1 kJ mol^{-1} and leads to a species, (int2+OH)/Pt_{10}, in which the OH fragment is adsorbed on the upper portion and between the two metal centers of a cluster edge.

For the removal of the OH species as water, a second H_2 molecule was fragmented on the cluster. The resulting species, (int2+OH)/Pt_{10}2H, is characterized by the presence of an H atom on an edge adjacent to the OH fragment and a second H atom on a far site of the cluster. The elementary stage in which this species becomes the reactant involves the transfer of an H atom to the O atom of the adsorbed fragment (energy barrier of 89.3 kJ mol^{-1}) with formation of chemisorbed H_2O (Figure S2a of ESI†). In order to proceed with the reaction, the H_2O molecule was desorbed from the cluster —desorption energy of 66.5 (BSSE = 5.4) kJ mol^{-1}— and the H atom, adsorbed and shared between two Pt atoms, diffused near the unsaturated C1. From the obtained species, int2/Pt_{10}H, origins thus the cyclohexane/Pt_{10} species, 9.2 kJ mol^{-1} more stable than its reactant, through the crossing of a low energy barrier, 54.7 kJ mol^{-1} (Figure S2b of ESI†). The resulting cyclohexane can desorb from the cluster with an energy of 89.6 (BSSE = 16.6) kJ mol^{-1}.

Pathway 2 suggests firstly the elimination of the −OH group as water and then the removal of the remaining oxygenated group as methanol, if C2-O bond breaking occurs, or methane, if O-CH_3 bond cleavage happens instead. In the latter case cyclohexane is obtained by removal of two water molecules. The early two elementary stages common to both bifurcations involve C1-O bond cleavage and methoxycyclohexane formation, respectively. Particularly, in the first elementary stage (Figure 4), there is, through the overcoming of an energy barrier of 157.7 kJ mol^{-1}, the breaking of the C1-O bond from 2-methoxycyclohexan-1-ol leading to a remarkable stabilization of the (int3+OH)/Pt_{10} system; the latter is characterized by the OH fragment adsorbed as bridge between two metal centers on an upper edge of the cluster, and the int3 showing O-Pt (bond length 2.22 Å) and C1-Pt (bond length 2.06 Å) interactions. The adsorbed OH, after fragmentation of an H_2 molecule on the cluster, can undergo hydrogenation hence desorption as water. In the second elementary step, from the int3/Pt_{10}H species, there is the transfer, characterized by an energy barrier of 102.7 kJ mol^{-1}, of an H atom to the unsaturated C1 of the ring with the formation of methoxycyclohexane/Pt_{10} —desorption energy of 128.8 (BSSE = 18.9) kJ mol^{-1}—, which is less stable than the intermediate that preceedes it by 48.4 kJ mol^{-1}. Methoxycyclohexane/Pt_{10} represents the species from which two alternative paths leading to cyclohexane are branched. According to one ramification (depicted in blue in Figure 4), the first elementary step includes, by crossing an energy barrier of 185.9 kJ mol^{-1}, the breakage of the C2-O bond with formation of the (int4+CH_3O)/Pt_{10} species, featuring the OCH_3 fragment adsorbed on the upper portion of the cluster edge. Following fragmentation of a new H_2 molecule on the cluster, the CH_3O could be hydrogenated to methanol and desorb. The resulting species, traceable to int2/Pt_{10}H from pathway 1, is hydrogenated on the unsaturated C2, giving cyclohexane. In the alternative bifurcation (shown in green in Figure 4), on the other hand, a slightly higher energy barrier (206.3 kJ mol^{-1}) is in the way for the O-CH_3 bond breaking. The (int5+CH_3)/Pt_{10} species, less stable by ca. 50 kJ mol^{-1} than the methoxycyclohexane/Pt_{10} species, exhibits a dangling oxygen atom interacting with the Pt atom at the apical position (O-Pt bond length of 1.89 Å) of the cluster and the adsorbed CH_3 fragment.

The last investigated route (pathway 3) involves the early elimination of methane (desorption energy equal to 23.4 kJ mol^{-1} with BSSE = 4.5 kJ mol^{-1}), which would lead to cyclohexane and two water molecules through the following formation of cyclohexane-1,2-diol and cyclohexanol. Overcoming an energy barrier of 161.0 kJ mol^{-1}, from the 2-methoxycyclohexan-1-ol there is an O-CH_3 bond scission leading to the (int6+CH_3)/Pt_{10} species (Figure 5). The latter, in addition to the CH_3 fragment being adsorbed on the Pt atom at the apical position, is characterized by two interactions, at the level of the oxygen atoms, with the adjacent metal centers of the upper portion of cluster edge. In the next elementary stage, due to fragmentation of an H_2 molecule on the cluster, methane generation occurs by transfer of an H

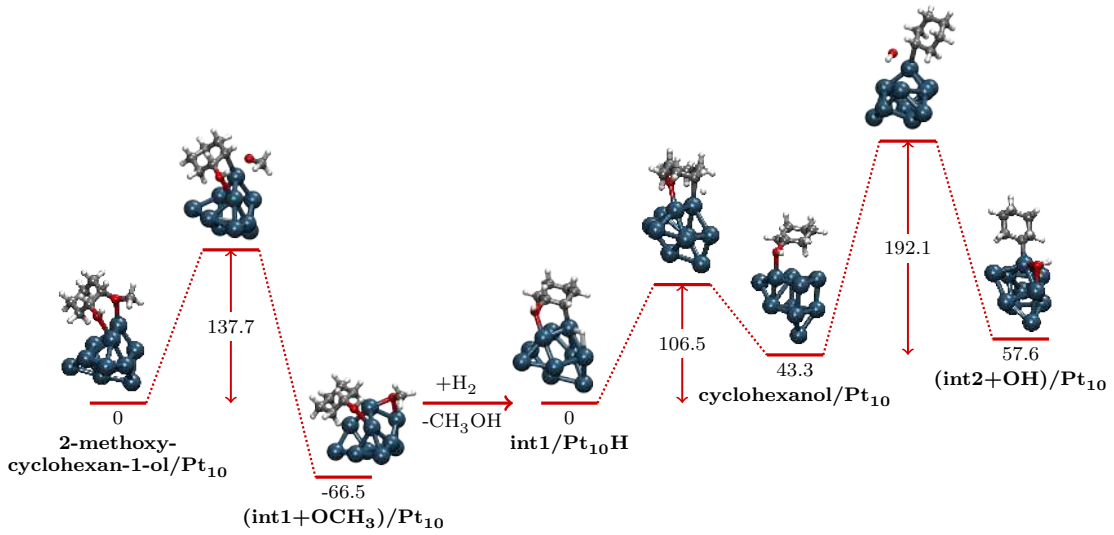

Fig. 3 Reaction profile showing C2-OCH_3 bond cleavage together with the shift of the CH_3O fragment on an edge of the cluster (HYD pathway 1). After addiction of H_2 molecule (which fragments on the cluster) and desorption of the methanol molecule, the formation of cyclohexanol with the subsequent cleavage of the C1-OH bond occur.

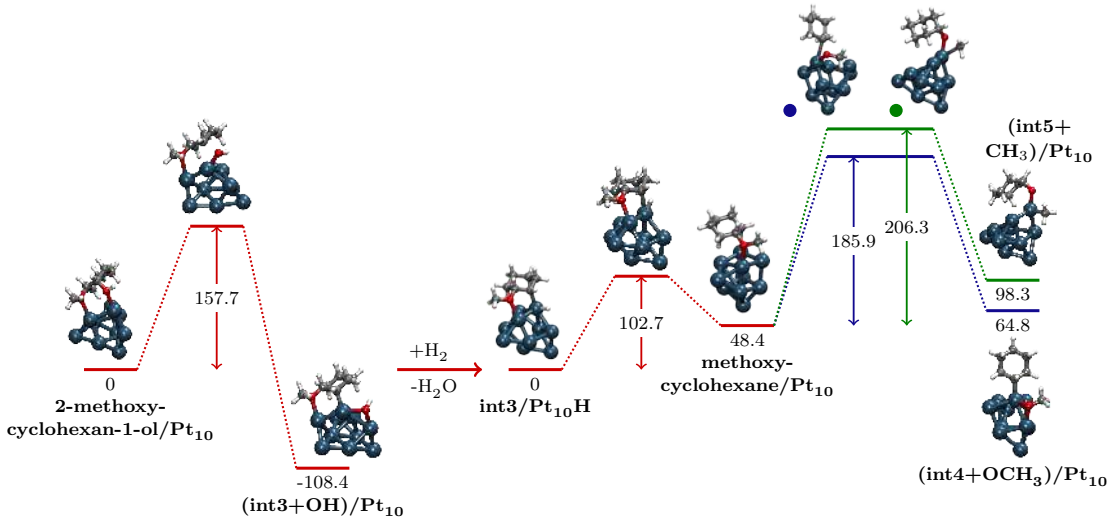

Fig. 4 Elementary steps related to the transformation on the platinum cluster of 2-methoxycyclohexan-1-ol to methoxycyclohexane and the OCH_3 loss from the latter (HYD pathway 2). The first step illustrates the breaking of C1-OH bond. After fragmentation of a new H_2 molecule on the cluster and the formation and desorption of water, the formation of methoxycyclohexane occurs through hydrogenation on C1. In the following steps the breaking of the C2-OCH_3 bond with the subsequent formation of methanol adsorbate (shown in blue), or the cleavage of the O-CH_3 bond in the methoxyl group to obtain methane (in green) is shown.

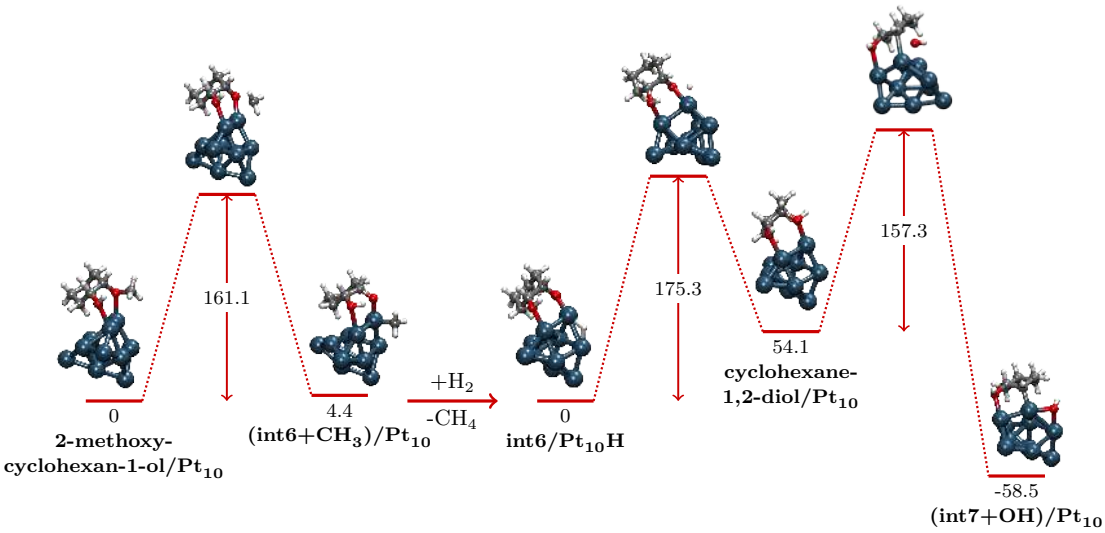

Fig. 5 The reaction profile according to the HYD pathway 3: after the O-CH_3 bond breaking in the methoxyl group, with the formation of the int6 and CH_3 species coadsorbed on Pt_{10}, methane desorbs following a H_2 molecule fragmentation. The formation of cyclohexan-1,2-diol/Pt_{10} occurs by hydrogenation of the dangling oxygen and is followed by the cleavage of the C2-OH bond.

atom to the C of the fragment. The subsequent desorption of methane and diffusion of the hydrogen atom through the cluster in the closeness of the dangling oxygen leads to the int6/$Pt_{10}H^b$ species, from which there is the formation of cyclohexane-1,2-diol/Pt_{10}. For this process, which requires oxygen atom hydrogenation, an energy barrier of 175.0 kJ mol^{-1} and a desorption energy of 94.3 (BSSE = 19.6) kJ mol^{-1} for cyclohexane-1,2-diol was calculated. From it, there is C2-O bond breakage (energy barrier 157.3 kJ mol^{-1}) with a considerable stabilization of the resulting species, (int7+OH)/Pt_{10}, in which the OH fragment is shared between two Pt atoms, and int7 interacts via O and the unsaturated C2 with two differently coordinated Pt atoms. As discussed for pathway 2, through the breaking of the C1-O bond (energy barrier: 192.1 kJ mol^{-1}), the removal of water and the saturation of C1 (energy barrier: 54.7 kJ mol^{-1} in Figure S2), cyclohexane is formed on Pt_{10} from cyclohexanol.

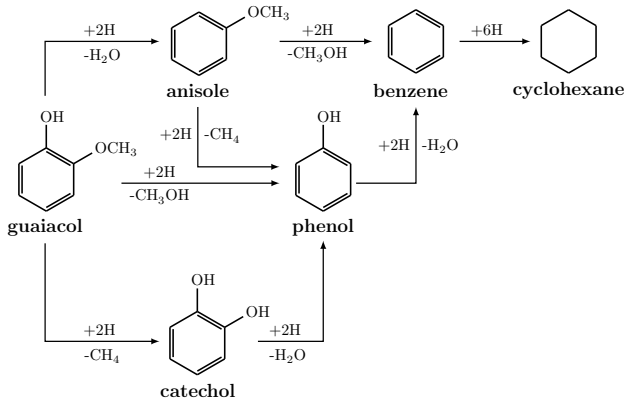

Scheme 2 Guaiacol conversion to cyclohexane according to DDO mechanism: schematic routes

3.2 DDO mechanism

The direct deoxygenation (DDO) mechanism of guaiacol involves firstly the removal of the oxygenated groups and then the hydrogenation of benzene to cyclohexane. Regarding deoxygenation, the order in which group removal can occur opens up different pathways, reported schematically in Scheme 2. If the first removed group is the −OH one the formation of anisole occurs (desorption energy 126.0 kJ mol^{-1}, with BSSE = 22.6 kJ mol^{-1}), from which two ramifications branch off to form benzene: one involves demethoxylation and the other a process of demethanation; in the latter case phenol can be formed. On the other hand, if the first group removed from guaiacol is the $-OCH_3$, phenol forms directly, which evolves to benzene. Alternatively, guaiacol could undergo demethanation to form catechol, which through the removal of two water molecules leads to the formation of benzene. The latter, generated from either one or more of the three proposed pathways, is subsequently hydrogenated to cyclohexane.

The first reaction pathway involves the elimination of the $-OCH_3$ group to obtain phenol which, through the removal of a water molecule, gives benzene. The initial elementary step of this channel (Figure 6) involves the cleavage of the C2-O bond (energy barrier of 129.2 kJ mol^{-1}) along with the migration of the OCH_3 fragment to a platinum atom, its hydrogenation and subsequent desorption. If a comparison is done with the demethoxylation energy barrier calculated by Lee *et al.*[59] for guaiacol on Pt(111), it turns out that when the platinum is reduced to subnanometric size the involved energy barrier can be sensibly lower. This occurrence, as well as other significant differences, can tentatively be explained taking into account the higher susceptibility to distortion of a cluster[60] with respect to the platinum surface.

It is now interesting to note that in the (int1′+OCH_3)/Pt_{10} species, the hydrogen bond, which is established between the hydroxyl H and methoxyl O centers, is reduced from 2.16 Å, (the length of the hydrogen bond in the guaiacol), to 1.60 Å. This

means that methanol formation occurs almost instantaneously by displacement of the hydroxyl H atom and without the intervention of hydrogen activated by the catalyst. In addition, the hydrogen bond length of 1.47 Å in the (int2′+CH_3OH)/Pt_{10} product suggests a near-sharing of the hydrogen atom between two oxygen atoms, probably favored by the small size of the metal cluster. Starting from the (int2′+CH_3OH)/Pt_{10} species, after fragmentation of a H_2 molecule on the cluster, the reaction continues with the restoration of the −OH group in the int2′. In order to deepen this aspect, it was decided to test to what extent the presence of methanol is able to influence this elementary stage by investigating the hydrogenation of dangling oxygen both with and without adsorbed methanol. In the former case, the energy barrier required for the conversion of (int2′+CH_3OH)/Pt_{10}2H to (int3′+CH_3OH)/Pt_{10}H is 49.9 kJ mol^{-1}, which is three times lower than that needed for the conversion of int2′/Pt_{10}2H to int3′/Pt_{10}H (167.1 kJ mol^{-1}), as illustrated in Figure S3 of ESI†. Furthermore, the hydrogenation of O atom in (int2′+CH_3OH)/Pt_{10}2H occurs with an energy release of 28.4 kJ mol^{-1}, to be compared with the 11.4 kJ mol^{-1} energy required for the same process in the absence of coadsorbed methanol. It is interesting here to observe the upshots related to the presence of the adsorbed methanol which apparently could be, at a first glance, thought of as a spectator species and which instead might locally act either electronically or sterically by inductive or proximity effects, respectively. The following hydrogen bond weakening, due to the restoration of the −OH group, facilitates methanol desorption. The resulting species, int3′/Pt_{10}H, undergoes hydrogenation on C2 (energy barrier of 63.3 kJ mol^{-1}) and the process is characterized by an energy release of 34.4 kJ mol^{-1} related to phenol/Pt_{10} formation. The calculated energy for phenol desorption is 132.8 (BSSE = 24.1) kJ mol^{-1}. However, for benzene to form, water must be removed. This requires overcoming an activation barrier of 96.4 kJ mol^{-1} for cleavage of the C1-O bond and obtaining the (int4′+OH)/Pt_{10} species that is more stable than phenol by about 30 kJ mol^{-1}. The adsorbed OH fragment is subsequently hydrogenated and removed as water; the adsorbed int4 species, on the other hand, is converted to benzene following hydrogenation of the unsaturated C1 carbon, a process characterized by a negligible energy barrier of 10.4 kJ mol^{-1} (Figure S4 of ESI†).

The second pathway proposed for the DDO mechanism involves the removal of the −OH group with the formation of anisole from which, either by loss of the $-OCH_3$ or of the $-CH_3$ fragment (in this case passing through phenol), benzene is obtained. We note here that the C-OCH_3 bond cleavage in anisole would be, again, a relatively easy step, opposite to the same process as it would occur for anisole in the Pt(111) surface.[54] It seems that also in this case the flexibility of the subnanometric cluster plays a fundamental role. In the transition state of this elementary process it can be indeed argued that the incipient phenyl radical which origins from the cleavage is stabilized by strong interactions with a distorted cluster. From benzene, by addition of three catalytically activated hydrogen molecules, cyclohexane is achieved. The first elementary stage of this pathway occurs by crossing an energy barrier of 163.9 kJ mol^{-1}, which is actually needed to break the C1−OH bond and thus obtain the (int5′+OH)/Pt_{10} species with the OH fragment adsorbed on a three-coordinate metal center of the cluster (Figure 7). The subsequent fragmentation of a new H_2 molecule triggers the formation and desorption of water, as well as the restoration of the system aromaticity. This process takes place in the second elementary stage in which, starting with the int5′/Pt_{10}H species, there is the transfer of an H atom to the unsaturated C1 of the ring with formation of anisole/Pt_{10}, which is more stable by about 29 kJ mol^{-1} than the intermediate reactant and for which the overcome of a relatively low energy barrier of 65.4 kJ mol^{-1} is required. Starting from the anisole/Pt_{10} species two mechanisms can take place. The C2-O bond breaking, characterized by an energy barrier of 70.2 kJ mol^{-1}, results in the formation of the (int6′+OCH_3)/Pt_{10} species. This, which is more stable than the chemisorbed anisole by 41 kJ mol^{-1}, has the OCH_3 fragment shared between two differently coordinated Pt atoms in the upper portion of an edge of the cluster. The fragment, following the dissociation of a H_2 molecule on the cluster, is hydrogenated to CH_3OH and desorbs. The resulting species, as already stated, readily undergoes hydrogenation on C2 giving a benzene molecule. Alternatively, there is the cleavage of the O-C bond in the $-OCH_3$ group, for which an energy barrier of 138.2 kJ mol^{-1} must be overcame; the obtained (int7′+CH_3)/Pt_{10} species is characterized by the CH_3 fragment on the Pt atom at the apical position and the presence of a dangling oxygen atom of the intermediate that interacts only via the ring carbons with the cluster. A hydrogen molecule dissociated on the cluster and hydrogenates the chemisorbed fragment to methane. This, following the desorption of the latter and the diffusion of the second H atom, leads to the int7′/Pt_{10}H species. From the latter, by the transfer of one H atom to the dangling O of the ring (energy barrier of 83.2 kJ mol^{-1}), chemisorbed phenol is formed, which, reconnecting with the first proposed pathway, leads to benzene/Pt_{10}.

The third pathway, finally, includes the removal of the methyl group as methane at the early stage with formation of the adsorbed catechol, from which by leakage of two water molecules benzene is obtained. The first elementary step of this proposed pathway involves cleavage of the O-CH_3 bond in the guaiacol/Pt_{10} with adsorption of the methyl fragment on a Pt atom of the cluster. For this species there is an energy release of 55.0 kJ mol^{-1}. This step is followed by hydrogenation of the chemisorbed fragment with formation of methane and its subsequent desorption. As a result of H atom diffusion through the cluster, there is hydrogenation of the dangling O atom in the int8′/Pt_{10}H (energy barrier of 155.8 kJ mol^{-1}) with the formation of catechol/Pt_{10}, which is 69.1 kJ mol^{-1} less stable than the reactant. From the catechol (whose desorption energy is 160.6 kJ mol^{-1}, with BSSE = 23.3 kJ mol^{-1}) there is the cleavage of the C2-OH bond with formation of the (int3′+OH)/Pt_{10} intermediate, where the -OH fragment is shared between two metal centers of a cluster edge (Figure 8). Subsequent removal of H_2O leads to the int3′/Pt_{10}H species, which leads to phenol/Pt_{10}, hence to benzene, as already discussed in the case of the first DDO pathway.

The benzene molecule obtained in the three DDO pathways

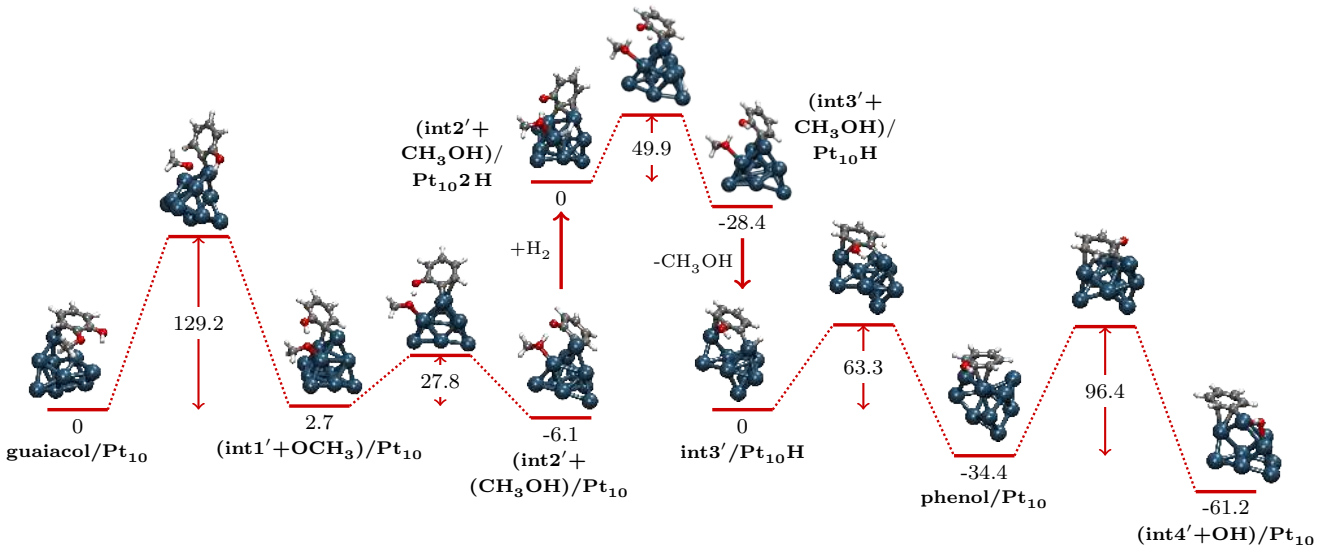

Fig. 6 The reaction profile corresponding to the DDO pathway 1: at first the cleavage of the C2-OCH_3 bond with the formation of the (int1′+OCH_3)/Pt_{10} species occurs along with intramolecular hydrogenation of the OCH_3 fragment. The hydrogenation, by catalyst-activated hydrogen, of the dangling O of int2′ in the presence of adsorbed CH_3OH follows. After, the desorption of methanol with the restoration of aromaticity gives phenol/Pt_{10}, while the subsequent cleavage of the C1-OH bond results in the (int4′+OH)/Pt_{10} species formation.

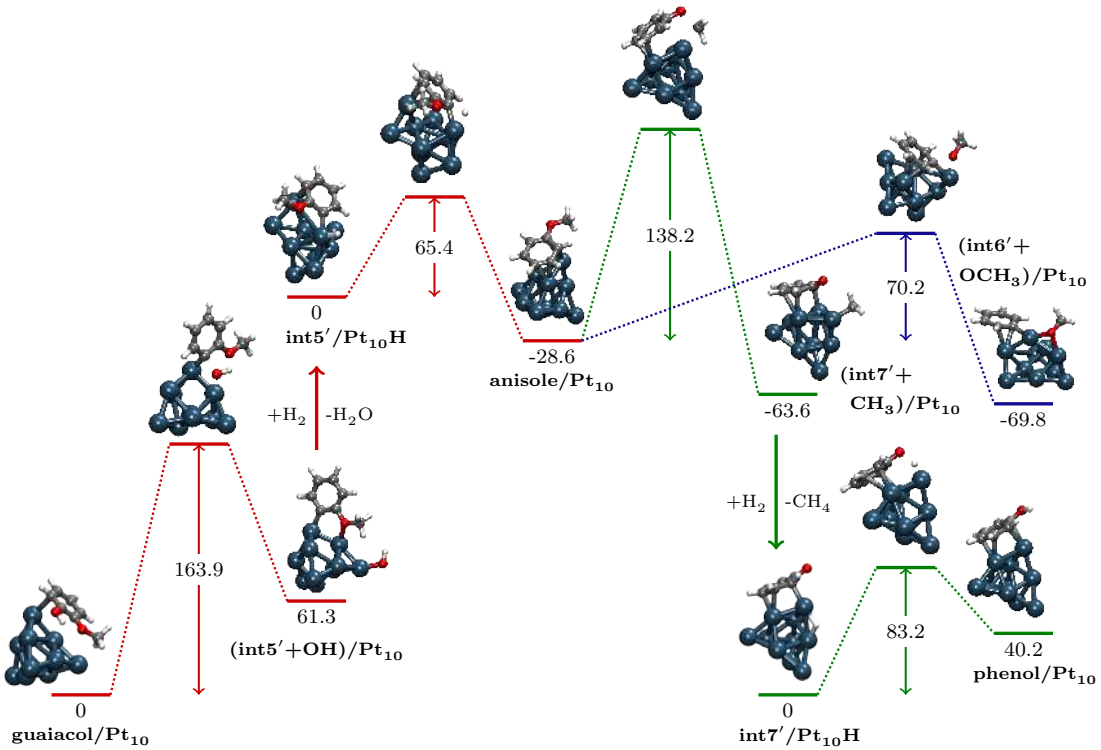

Fig. 7 Elementary steps for the second DDO pathway: the cleavage of C1-OH bond from guaiacol/Pt_{10} gives the (int5′+OH)/Pt_{10} species that, after a H_2 molecule intervention and water desorption, is transformed to anisole/Pt_{10} through the restoration of the phenyl ring. The latter can follow two paths: the C-OCH_3 bond breaking, which gives ultimately raise to methanol and benzene (blue lines) or the OC-CH_3 bond breaking, which instead produces methane, benzene and water (green lines), through phenol as intermediate species.

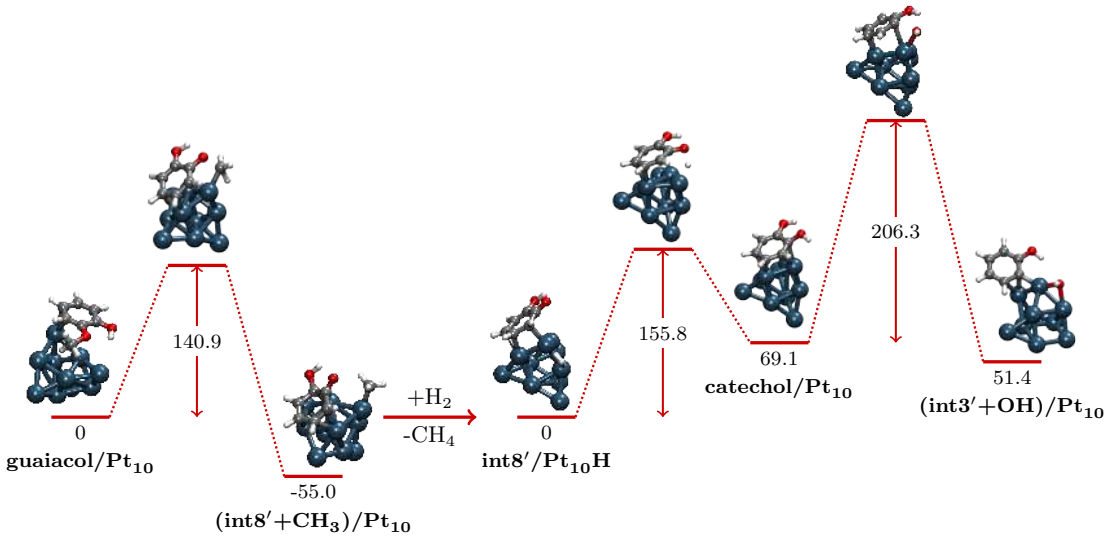

Fig. 8 DDO pathway 3: methane and catechol formation from guaiacol. Catechol/Pt_{10} will then loose water and trasnform to a phenol precursor through C2-OH bond cleavage.

(which could desorb with an energy of 167.5 kJ mol^{-1}, BSSE = 26.4 kJ mol^{-1}) must be transformed, by consecutive hydrogenations, to cyclohexane. Whereas in the HYD mechanism there is the combination of two factors (the electronic effects of substituents and the metal/substrate interactions) complicating the choice of the favorite site for hydrogenation, in this case the addition of the first hydrogen atom is governed only by the presence of the metal/substrate interactions. On this basis, the only carbon atoms available to hydrogenation are those for which interaction with Pt atoms in the cluster occurs. In view of this, the addition of the first hydrogen atom was only considered on four carbon atoms of the ring, numbered as 1, 2, 5 and 6 in Figure 9. C6 is the carbon atom that preferentially undergoes hydrogenation by virtue of its lower energy barrier (82.4 kJ mol^{-1}) with respect to the alternative sites and the higher stability of the obtained intermediate. For subsequent hydrogenations, as mentioned above, carbon atoms in the *ortho*- position with respect to the pre-existing H atom(s) are identified as potential sites for hydrogenation. The carbon atoms, *ortho* to C6, on which the addition of the second H atom was considered are thus 1 and 5. The lower energy barrier (83.6 vs. 103.4 kJ mol^{-1}) suggests that hydrogenation takes place preferentially on C5, leading to cyclohexa-1,3-diene (desorption energy of 190.9 kJ mol^{-1} with BSSE = 24.1 kJ mol^{-1}). From it, the addition of a third H atom to C4 (very low energy barrier of 24.9 kJ mol^{-1}) results in an energy release of 22.1 kJ mol^{-1} due to the formation of the intermediate species **IIIa**. Then, following the transfer of an H atom to C3, there is the formation of the stable cyclohexene species, for which a desorption energy of 154.2 kJ mol^{-1} with BSSE =21.6 kJ mol^{-1} was calculated. On the basis of lower activation energy (35.4 vs 85.9 kJ mol^{-1}) and higher relative stability of the intermediate involved (17.6 vs 40.1 kJ mol^{-1}), the C2 is considered the favored site for the addition of the fifth H atom and, finally, the **Va** intermediate undergoes hydrogenation on C1 leading to the formation of the adsorbed cyclohexane. The calculated desorption energy for cyclohexane finally resulted

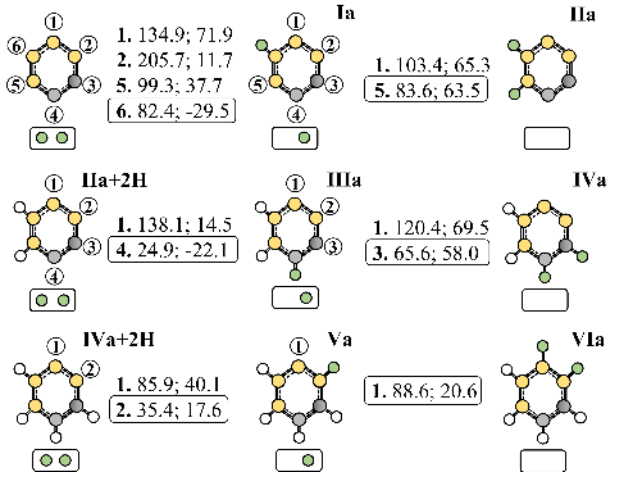

Fig. 9 Representation of the complete saturation of benzene on the Pt_{10} cluster. The yellow circles indicate the interaction sites of the molecule with the cluster, which is instead represented by a small rectangle containing the adsorbed hydrogen atoms (green circles). To the right of each species, the first number indicates the position where the catalytic hydrogen is added, the second is the energy barrier of the corresponding elementary step, and the third is the energy of the product referred to its reactant. All energy values are expressed in kJ mol^{-1}. The first catalytic hydrogenation starts from benzene, the second from IIa+2H (cyclohexa-1,3-diene), the last from IVa+2H (cyclohexene).

equal to 85.0 kJ mol^{-1} with BSSE = 17.6 kJ mol^{-1}.

3.3 Kinetic analysis

In the previous sections we discussed eight possible mechanisms for the conversion of guaiacol to cyclohexane on the Pt_{10} cluster, which are summarized in Schemes 1 and 2. The results of DFT calculations comprise energy barriers and relative energies of minima on the potential energy surface. These results would indicate that, in the early stage of the reaction, the hydrogena-

tion of the phenyl ring would be kinetically favored with respect to deoxygenation, but this latter would have higher probability to occur just from guaiacol instead of the full hydrogenated product, methoxycyclohexanol. In order to better discriminate the fastest mechanism we used a microkinetic analysis instead of basing our conclusions on the inspection of energy barriers. In particular, the Simplified Christiansen Method (SCM) recently developed and described in[23,61] was employed. Since the desorption of the final product, cyclohexane, is significantly affected by entropy variation and, in turn, affects the rate of the whole reaction, the SCM analysis was performed in terms of Gibbs free energies as a function of the temperature. As it can be concluded from Tables S1-S3 of ESI†, the use of ΔG instead of E_{ZPV} has a negligible effect on the barriers and intermediate energy differences, but has indeed a major influence on the desorption energies of all stable intermediates.

The results of the SCM analysis, whose details are reported in Tables S4-S7 of Supporting Information†, indicated that the DDO channels are always at least two orders of magnitude faster than those present in the HYD pathways. In particular, the DDO routes involving the formation of anisole and phenol share the same reaction rate in the lowest part of the temperature range, being the benzene hydrogenation the slowest process. At higher temperatures the HDO reaction on Pt_{10} seems to proceed essentially through the first DDO pathway, the one involving the formation of intermediate phenol originated by early demethoxylation. The DDO channel passing through catechol has lower reaction rates since it involves the high reaction barrier corresponding to the C−OH bond cleavage. Since the fastest mechanisms are of DDO type and benzene reduction is slow, the benzene molecule is the one showing the higher surface molar ratio Θ at all the considered temperatures (from 473 to 1073 K).

The HYD channel passing through methoxycyclohexane, which directly transforms to cyclohexane, is slightly preferred over the other pathways. The analysis indicated that the C-OH cleavage in 2-methoxycyclohexa-1-ol (product of the phenyl ring hydrogenation of guaiacol) is slightly favored with respect to the C-OCH3 one and that, conversely, the O-CH3 bond breaking, to ultimately form methane, is always the less favored process. However, all HYD routes but the one involving methane production have essentially the same reaction rate. According to what was anticipated on the basis of energy barriers (for the sake of comparison, the SCM-calculated reaction rates at various temperatures in terms of E_{ZPV} are reported in Table S7), the full reduction of phenyl ring in guaiacol is a kinetically easy process, but the rate of the HYD mechanisms are negatively affected by the slow process corresponding to the C-O cleavage.

4 Conclusions

The present investigation, framed in the context of the constant demand for renewable and eco-sustainable alternatives, aims to provide an atomistic-level analysis of the "direct deoxygenation" (DDO) and "deoxygenation-through-hydrogenation" (HYD) mechanisms for the hydrodeoxygenation reaction of guaiacol catalized by a subnanometric platinum cluster. Although several experimental and computational studies suggest the predominance of a mechanism rather than another depending on the metal used (as an example, noble or non-noble), this may not be true in the investigated catalytic model since processes on subnanometer clusters do not necessarily follow the established rules of heterogeneous catalysis and, conversely, represent a chemistry to be investigated case by case. For this reason, both mechanisms have been studied being the observations deduced from the DFT calculations and the SCM analysis of the results are summarized below.

Even if the early hydrogenation of the phenyl ring in guaiacol would be faster than the homolytic cleavage of $C(sp^2)$-O bonds, on Pt_{10} the DDO mechanisms is favored with respect to the HYD one. This because the energy barriers for the breaking of both the $C(sp^2)$-OCH_3 bond from guaiacol and the $C(sp^2)$-OH bond from phenol result substantially lower than for the breaking of the $C(sp^3)$-OCH_3 bonds in 2-methoxycyclohexan-1-ol and $C(sp^3)$-OH bonds in cyclohexanol. In addition, the energy barrier related to the cleavage of the $C(sp^2)$-OCH_3 bond of anisole is lower than the corresponding barrier in the fully hydrogenated equivalent occurring in the HYD mechanism. At 0 K, the desorption energies related to the molecular species cyclohexanol and methoxycyclohexane are lower than the amount of energy required to overcome the energy barriers for the elementary stages of $C(sp^3)$-OH and $C(sp^3)$-OCH_3 bond cleavage, which are necessary for the reaction to proceed. In contrast, in the DDO mechanism the desorption of molecular species is more difficult; the amount of energy calculated for the species desorption is always greater than the energy barrier for the following elementary stage of the reaction. These evidences can be attributed to the interaction of the substrate with Pt: in the DDO mechanism, the aromatic species shows considerable interactions with the cluster through the phenyl ring, which makes it easier to break the C-O bonds; in the HYD mechanism, on the other hand, the hydrogenated species are weakly adsorbed. Consequently, it can be inferred that in the HYD mechanism only a negligible percentage of molecules will be able to cross the energy barriers necessary for the reaction progress and thus only a very small fraction of it will succeed in yielding the desired cyclohexane as final product. For the HYD channels the same conclusions hold true at low temperatures if the reaction energetic is formulated in terms of Gibbs free energies, while in the DDO cases desorption and transformations become competitive. At higher temperatures desorption phenomena occur more easily but, according to the microkinetic analysis, the net effect is always a preference for the DDO mechanism. In particular, in the preferred pathway the elimination of the $-OCH_3$ group as methanol is followed by the elimination of the $-OH$ group as water.

Author Contributions

Chiara Nania: Investigation, Data curation, Writing - original draft; Marco Bertini: Investigation, Data curation, Methodology; Laura Gueci: Investigation, Data curation; Francesco Ferrante: Conceptualization, Methodology, Data curation, Writing, Supervision; Dario Duca: Supervision, Project administration.

Conflicts of interest

There are no conflicts to declare.

Notes and references

1 D. C. Elliott, *Advances in Bioenergy*, John Wiley & Sons, Ltd, 2016, pp. 65–72.

2 R. Ahorsu, F. Medina and M. Constantí, *Energies*, 2018, **11**, 1–19.

3 M. N. Uddin, K. Techato, J. Taweekun, M. M. Rahman, M. G. Rasul, T. M. I. Mahlia and S. M. Ashrafur, *Energies*, 2018, **11**, 3115.

4 A. Bjelic, M. Grilc, M. Hus and B. Likozar, *Chem. Eng. J.*, 2019, **359**, 305–320.

5 A. Bridgwater, *Biomass and Bioenergy*, 2012, **38**, 68–94.

6 *Renewable Energy: Power for a Sustainable Future (3rd ed.)*, 2012, Published by Oxford University Press, Oxford in association with The Open University, Milton Keynes.

7 A. Bridgwater, *Chem. Eng. J.*, 2003, **91**, 87–102.

8 D. C. Elliott, *Curr. Opin. Chem. Eng.*, 2015, **9**, 59–65.

9 M. Bertero, G. de la Puente and U. Sedran, *Fuel*, 2012, **95**, 263–271.

10 J. Feng, C.-y. Hse, Z. Yang, K. Wang, J. Jiang and J. Xu, *Appl. Catal. A: Gen.*, 2017, **542**, 163–173.

11 D. Mohan, C. U. Pittman and P. H. Steele, *Energy Fuels*, 2006, **20**, 848–889.

12 D. Gao, Y. Xiao and A. Varma, *Ind. Eng. Chem. Res.*, 2015, **54**, 10638–10644.

13 F. E. Massoth, P. Politzer, M. C. Concha, J. S. Murray, J. Jakowski and J. Simons, *J. Chem. Phys. B*, 2006, **110**, 14283–14291.

14 L. Bomont, M. Alda-Onggar, V. Fedorov, A. Aho, J. Peltonen, K. Eränen, M. Peurla, N. Kumar, J. Wärnå, V. Russo, P. Mäki-Arvela, H. Grénman, M. Lindblad and D. Y. Murzin, *Eur. J. Inorg. Chem.*, 2018, **2018**, 2841–2854.

15 L. Nie and D. E. Resasco, *J. Catal.*, 2014, **317**, 22–29.

16 M. Hellinger, H. W. Carvalho, S. Baier, D. Wang, W. Kleist and J.-D. Grunwaldt, *Appl. Catal.s A Gen.*, 2015, **490**, 181–192.

17 H. Lee, H. Kim, M. Yu, C. H. Ko, J.-K. Jeon, J. Jae, S. Park, S.-C. Jung and Y.-K. Park, *Sci. Rep*, 2016, **6**, 28765.

18 A. Bjelić, M. Grilc and B. Likozar, *Chem. Eng. J.*, 2018, **333**, 240–259.

19 A. Prestianni, F. Ferrante, E. M. Sulman and D. Duca, *J. Phys. Chem. C*, 2014, **118**, 21006–21013.

20 F. Ferrante, A. Prestianni, M. Bertini and D. Duca, *Catalysts*, 2020, **10**, 1306.

21 F. Ferrante, A. Prestianni, R. Cortese, R. Schimmenti and D. Duca, *J. Phys. Chem. C*, 2016, **120**, 12022–12031.

22 K. Koichumanova, A. K. K. Vikla, R. Cortese, F. Ferrante, K. Seshan, D. Duca and L. Lefferts, *Appl. Catal. B Env.*, 2018, **232**, 454–463.

23 L. Gueci, F. Ferrante, A. Prestianni, F. Arena and D. Duca, *Mol. Catal.*, 2021, **513**, 111735.

24 C. González, P. Marín, F. V. Díez and S. Ordóñez, *Ind. Eng. Chem. Res.*, 2016, **55**, 2319–2327.

25 C. Liu, H. Tao, C. Lian and H. Liu, *T. Phys. Chem. C*, 2022, **126**, 9724–9735.

26 S. Tieuli, P. Mäki-Arvela, M. Peurla, K. Eränen, J. Wärnà, G. Cruciani, F. Menegazzo, D. Y. Murzin and M. Signoretto, *Appl. Catal. A: Gen.*, 2019, **580**, 1–10.

27 P. Mäki-Arvela and D. Y. Murzin, *Catalysts*, 2017, **7**, 265.

28 C. Lindfors, P. Mäki-Arvela, P. Paturi, A. Aho, K. Eränen, J. Hemming, M. Peurla, D. Kubička, I. L. Simakova and D. Y. Murzin, *ACS Sustain. Chem. Eng.*, 2019, **7**, 14545–14560.

29 M. Alda-Onggar, P. Mäki-Arvela, K. Eränen, A. Aho, J. Hemming, P. Paturi, M. Peurla, M. Lindblad, I. L. Simakova and D. Y. Murzin, *ACS Sustain. Chem. Eng.*, 2018, **6**, 16205–16218.

30 M. Alda-Onggar, P. Mäki-Arvela, A. Aho, I. Simakova and D. Murzin, *React. Kinet. Mech. Catal.*", 2019, **126**, 737–759.

31 C. Zhao, S. Kasakov, J. He and J. A. Lercher, *J. Catal.*, 2012, **296**, 12–23.

32 L. Gueci, F. Ferrante, A. Prestianni, R. Di Chio, A. F. Patti, D. Duca and F. Arena, *Inorg. Chim. Acta*, 2020, **511**, 119812.

33 F. Arena, F. Ferrante, R. Di Chio, G. Bonura, F. Frusteri, L. Frusteri, A. Prestianni, S. Morandi, G. Martra and D. Duca, *Appl. Cat. B Env.*, 2022, **300**, 120715.

34 V. D'Anna, D. Duca, F. Ferrante and G. La Manna, *Phys. Chem. Chem. Phys.*, 2010, **12**, 1323–30.

35 R. Schimmenti, R. Cortese, F. Ferrante, A. Prestianni and D. Duca, *Phys. Chem. Chem. Phys.*, 2016, **18**, 1750–1757.

36 R. B. King, *Applications of graph theory and topology in inorganic cluster and coordination chemistry / R. Bruce King.*, CRC Press, 1993.

37 I. Demiroglu, K. Yao, H. A. Hussein and R. L. Johnston, *J. Chem. Phys. C*, 2017, **121**, 10773–10780.

38 M. Brack, *Sci. Am.*, 1997, **277**, 50–55.

39 G. Barone, D. Duca, F. Ferrante and G. La Manna, *Int. J. Quant. Chem.*, 2010, **110**, 558–562.

40 F. Ferrante, C. Nania and D. Duca, *Mol. Catal.*, 2022, **529**, 112541.

41 J. A. Maga and I. Katz, *Crit. Rev. Food Sci. Nutr.*, 1978, **10**, 323–372.

42 A. M. Verma and N. Kishore, *Royal Society Open Science*, 2017, **4**, 170650.

43 J. Lu, S. Behtash, O. Mamun and A. Heyden, *ACS Catal.*, 2015, **5**, 2423–2435.

44 K. Lee, G. H. Gu, C. A. Mullen, A. A. Boateng and D. G. Vlachos, *ChemSusChem*, 2015, **8**, 315–322.

45 D. Gao, C. Schweitzer, H. T. Hwang and A. Varma, *Ind. Eng. Chem. Res.*, 2014, **53**, 18658–18667.

46 M. J. Frisch, G. W. Trucks, H. B. Schlegel, G. E. Scuseria, M. A. Robb, J. R. Cheeseman, G. Scalmani, V. Barone, G. A. Petersson, H. Nakatsuji, X. Li, M. Caricato, A. V. Marenich, J. Bloino, B. G. Janesko, R. Gomperts, B. Mennucci, H. P. Hratchian, J. V. Ortiz, A. F. Izmaylov, J. L. Sonnenberg, D. Williams-Young, F. Ding, F. Lipparini, F. Egidi, J. Goings, B. Peng, A. Petrone, T. Henderson, D. Ranasinghe, V. G. Zakrzewski,

J. Gao, N. Rega, G. Zheng, W. Liang, M. Hada, M. Ehara, K. Toyota, R. Fukuda, J. Hasegawa, M. Ishida, T. Nakajima, Y. Honda, O. Kitao, H. Nakai, T. Vreven, K. Throssell, J. A. Montgomery, Jr., J. E. Peralta, F. Ogliaro, M. J. Bearpark, J. J. Heyd, E. N. Brothers, K. N. Kudin, V. N. Staroverov, T. A. Keith, R. Kobayashi, J. Normand, K. Raghavachari, A. P. Rendell, J. C. Burant, S. S. Iyengar, J. Tomasi, M. Cossi, J. M. Millam, M. Klene, C. Adamo, R. Cammi, J. W. Ochterski, R. L. Martin, K. Morokuma, O. Farkas, J. B. Foresman and D. J. Fox, *Gaussian~16 Revision C.01*, 2016.

47 A. D. Becke, *J. Chem. Phys.*, 1993, **98**, 1372–1377.

48 S. Grimme, J. Antony, S. Ehrlich and H. Krieg, *J. Chem. Phys.*, 2010, **132**, 154104.

49 P. J. Hay and W. R. Wadt, *J. Chem. Phys.*, 1985, **82**, 270–283.

50 P. J. Hay and W. R. Wadt, *J. Chem. Phys.*, 1985, **82**, 299–310.

51 T. H. Dunning and P. J. Hay, *Methods of Electronic Structure Theory*, Springer US, 1977, pp. 1–27.

52 B. P. Pritchard, D. Altarawy, B. Didier, T. D. Gibson and T. L. Windus, *J. Chem. Inf. Model.*, 2019, **59**, 4814–4820.

53 S. F. Boys and F. Bernardi, *Mol. Phys.*, 1970, **19**, 553–566.

54 R. Réocreux, C. A. Ould Hamou, C. Michel, J. B. Giorgi and P. Sautet, *ACS Catal.*, 2016, **6**, 8166–8178.

55 A. M. Verma and N. Kishore, *Chem. Select*, 2016, **1**, 6196–6205.

56 M. Saeys, M.-F. Reyniers, M. Neurock and G. B. Marin, *J. Phys. Chem. B*, 2005, **109**, 2064–2073.

57 T. Bera, J. W. Thybaut and G. B. Marin, *Ind. Eng. Chem. Res.*, 2011, **50**, 12933–12945.

58 L. Lozano, G. B. Marin and J. W. Thybaut, *Ind. Eng. Chem. Res.*, 2017, **56**, 12953–12962.

59 K. Lee, G. H. Gu, C. A. Mullen, A. A. Boateng and D. G. Vlachos, *ChemSusChem*, 2015, **8**, 315–322.

60 H. Zhai and A. N. Alexandrova, *ACS Catal.*, 2017, **7**, 1905–1911.

61 L. Gueci, F. Ferrante, A. Prestianni, F. Arena and D. Duca, *Data in Brief*, 2021, **38**, 107369.